Test of a Conceptual Prototype of the
Total Internal Reflection Cherenkov Imaging Detector (DIRC)
with Cosmic Muons*

D. Aston,[a] C. Hearty,[b] J. Kadyk,[c] H. Kawahara,[a][†] A. Lu,[d] G. Lynch,[c]
D. McShurley,[a] B. Meadows,[e] D. Muller,[a] G. Oxoby,[a] W. Pope,[c] M. Pripstein,[c]
B. Ratcliff,[a] R. Reif,[a] C. Simopoulos,[a] M. Smy,[f] H. Staengle,[f] P. Stiles,[a]
M. Z. Wang,[g] D. Warner,[f] W. Wenzel,[c] R. J. Wilson,[f] S. Yellin,[d] Y. Zhu[a]

[a]Stanford Linear Accelerator Center, Stanford, CA 94309, USA

[b]Department of Physics, University of British Columbia, Vancouver, BC V6T 2A6, Canada

[c]Lawrence Berkeley Laboratory, University of California, Berkeley, CA 94720, USA

[d]Department of Physics, University of California, Santa Barbara, CA 93106, USA

[e]Department of Physics, University of Cincinnati, Cincinnati, OH 45221, USA

[f]Department of Physics, Colorado State University, Fort Collins, CO 80523, USA

[g]Department of Physics and Astronomy, University of Iowa, Iowa City, IA 52242, USA

Abstract

The DIRC is a totally internally reflecting Cherenkov imaging detector proposed for particle identification at the asymmetric e^+e^- B factories. First test results from a conceptual prototype using cosmic muons are reported. The photo-electron yield and the single Cherenkov photon resolution at various track dip angles and positions along the radiator bar have been measured. The results are consistent with estimates and Monte-Carlo simulations.

I.   Introduction

An excellent charged particle identification system is essential for a general purpose detector at an asymmetric e^+e^- B factory [?, ?]. Measurements of CP violation require particle identification to tag the flavor of B mesons and to reconstruct exclusive final states. The momentum distribution of particles from B decays extends above 4 GeV/c due to the boost along the e^- beam direction with the fastest particles going at large forward dip angles. While electrons and muons can be identified by the electromagnetic calorimeter and the muon system, there is no easy way of identifying charged hadrons. Conventional technology such as a combination of dE/dx measurement in the tracking chamber and a time-of-flight system would require a very large detector size to cover the whole momentum range with good separation, while Cherenkov based techniques require further development [?].
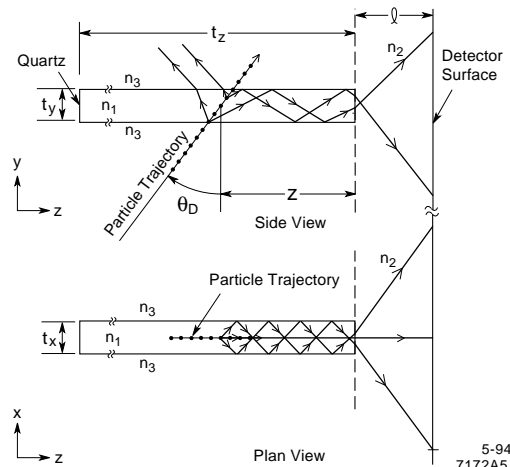

Figure 1: Imaging principle of the DIRC.

The DIRC is a new kind of Cherenkov imaging device which utilizes totally internally reflecting Cherenkov photons in the visible and near UV range [?]. It is thin (in both size and radiation length), robust, very fast, and expected to have excellent performance over the entire momentum range of the B factory.

II.   Imaging Principle

The geometry of the DIRC is shown schematically in Fig. ??. It utilizes a long, thin, flat quartz radiator bar (effective mean refractive index $n_1 = 1.474$) with rectangular cross section. The radiator bar is surrounded by a material with a small refractive index $n_3 \sim 1$ (air in this
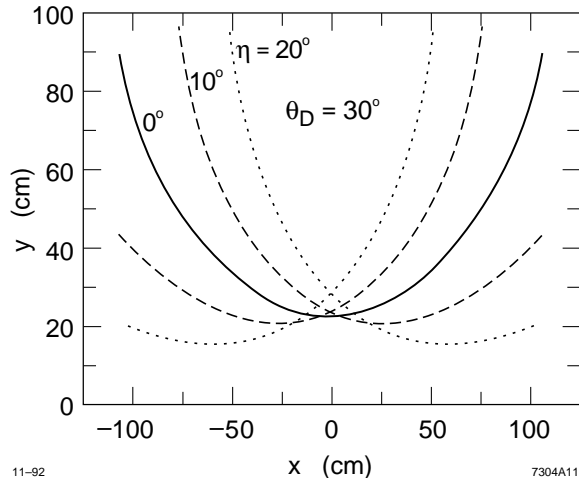
Figure 2: Loci of Cherenkov images from a $\beta = 1$ track on a detection surface at 100 cm from the radiator bar end. Only the upper half of the image is shown. The images are shown for a dip angle θ_D of 30° and three different azimuthal angles η.

Figure 3: Schematic view of one quadrant of a model B factory detector incorporating a DIRC. The stand-off box has reflective surfaces to save PMTs.

case). For particles with $\beta = 1$, since the index of the radiator bar n_1 is larger than $\sqrt{2}$, some of the Cherenkov photons will be totally internally reflected, regardless of the incidence angle of the tracks. The photons are then transported along the bar to the end. Since the bar has a rectangular cross section, the direction of the photons remains unchanged during the transport, except for left-right/up-down ambiguities due to the reflection at the radiator bar surfaces. The photons are then proximity focused by expanding through a stand-off region (index n_2) onto the photon detection surface placed at a distance l from the bar end. Fig. **??** shows the upper half of the image. The lower half is symmetric about the x-axis. The image is essentially a section of the Cherenkov cone. For tracks with azimuthal angle $\eta \neq 0$, the locus of the image is split into two lines due to the left-right ambiguity. The index of the stand-off region material n_2 should be close to that of the radiator n_1 to maximize the transfer efficiency through the bar end [**?**]. Water is the current choice due to its reasonable cost, long photon absorption length, and low relative chromatic dispersion when matched with quartz.

Fig. **??** shows a possible arrangement of a B factory detector with a DIRC. Since the photons are transported along the radiator bar, the photon detector can be placed outside the magnetic field. The natural choice for the detector is a closely packed array of Photo-Multiplier Tubes (PMTs). PMTs are fast, robust, easy to use, commercially available at modest cost, and have high gain to allow use of simple electronics. They also have very good time resolution which helps to reject backgrounds. Typical PMTs with bialkali photo-cathodes and borosilicate glass windows are sensitive to photons of wavelength be-
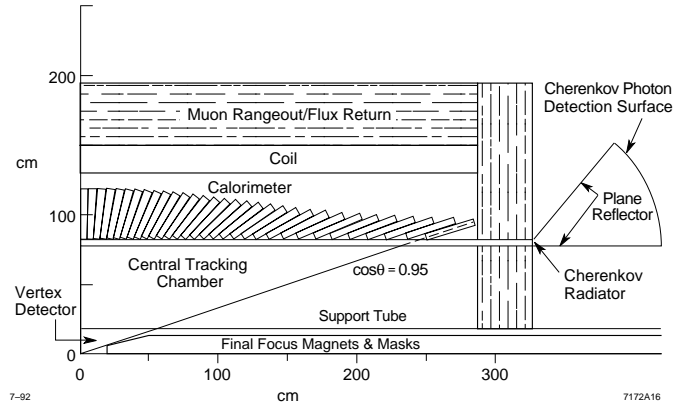
tween 300 and 600 nm, where quartz has a long absorption length and small chromatic dispersion.

The DIRC has several major advantages. It uses completely conventional components, such as PMTs and quartz bars, whose properties are well-understood and can be reliably simulated. Because it uses Cherenkov photons trapped by total internal reflection, unlike other Cherenkov imaging devices, the performance improves as the track dip angle increases. This is an advantage at an asymmetric e^+e^- B factory, where the tracks are boosted toward the forward hemisphere and have higher momentum at larger dip angles. It also occupies a small radial space (~ 8 cm), so the overall detector size and cost can be reduced significantly.

III.   Conceptual Prototype

Although the concept of the DIRC is straightforward, prototype testing is important to understand the device fully and to avoid possible surprises. The main goals of the conceptual prototype are to measure the number of Cherenkov photo-electrons observed from fast tracks as a function of track dip angle and position along the bar, and to measure the single Cherenkov photon angle resolution. We also need to examine the feasibility of gluing quartz bars, since $\sim$5 m long bars are needed for the full scale detector and producing bars of this length without joints seems impractical.

Fig. **??**. shows the cosmic ray test apparatus. We tested 120 cm and 240 cm long quartz bars (Vitreosil 055)[1], 4.73 cm wide and 1.70 cm thick. The 240 cm long bar is made from two 120 cm long bars glued together with an epoxy[2] which has good transmission at wavelengths to
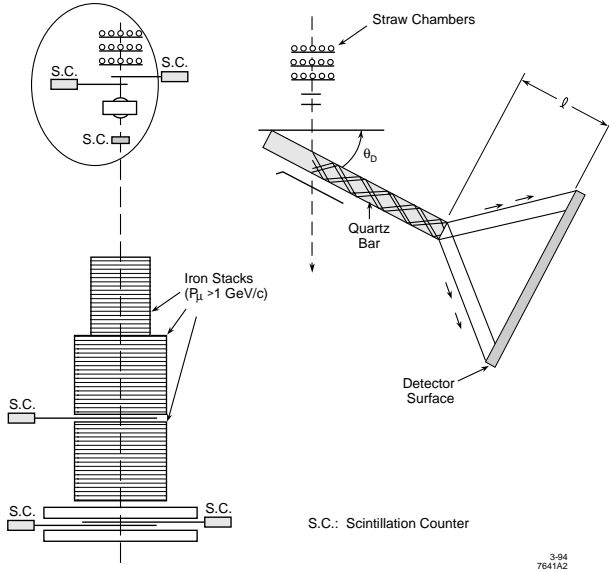
Figure 4: The DIRC conceptual prototype. The photon detector is a single PMT at the bar end or an array of PMTs at the detector surface.

Figure 5: The observed photo-electron yield from a 1.7 cm thick bar at a track position $z = 60$ cm as a function of dip angle θ_D. The solid line is a Monte-Carlo simulation. The statistical errors of the measurements are smaller than the circles. There is a scale error of 3 % due to calibration uncertainty.

which the PMTs are sensitive. The quartz bars are placed in a light-tight box and supported by a few sets (3 for 120 cm, 4 for 240 cm long bar) of nylon screws to minimize contact with the bar surface. The light loss due to this contact is negligible. The light-tight box is mounted on rotating rails to allow angle and position variation.

The cosmic muon trigger is provided by scintillation counters with an angular acceptance of $\pm 6.5°$ from the vertical in both directions. A 1 GeV/c threshold is provided by an iron stack underneath the bar. The Cherenkov angle variation due to the momentum distribution of the muons is 1.6 mr (RMS), which is small compared with the total angular resolution. An array of straw chambers is used to measure the track direction for the single Cherenkov photon angle resolution measurement.

To measure the photo-electron yield, single 2″ diameter PMTs (Burle-8850[3]) are directly glued to the end of each bar. To measure the angular resolution, a closely packed array of 47 $1\frac{1}{8}″$ diameter PMTs (EMI-9124A[4], minimum effective cathode diameter 2.3 cm) is used. The stand-off region material is air to allow easy movement of the array. Since the array is only 27 cm wide and 12 cm high, it covers a small portion of the image. Both types of PMT have bialkali photo-cathodes. The cathode blue sensitivity of the Burle-8850's used for the photo-electron yield measurement is 10.0 μA/lm for the 120 cm long bar and 9.7 μA/lm for the 240 cm long bar. The typical cathode blue sensitivity of an EMI-9124A is 11 μA/lm. Both types

of PMT have linear focused dynodes and good single photon response.

A number of properties of the bars have been examined in an optical test setup. In particular, laser measurements demonstrate that the photon absorption length is greater than 30 m, and the internal reflection coefficient exceeds 0.999. The light loss in the 240 cm long bar, which has a glue joint, is about 4 % at $\lambda = 325$ nm and less than the sensitivity of the measurement at $\lambda = 442$ nm.

IV. RESULTS

A. *Photo-electron Yield*

Fig. **??** shows the observed average number of photo-electrons as a function of track dip angle. The measurements were performed on the 120 cm long bar and the track position z was 60 cm from the PMT end of the bar. The gain of the PMT was calibrated by thermal electrons from the photo-cathode. The calibration error is 3 %, mainly due to the uncertainty of the ADC pedestal. The solid line is a Monte-Carlo simulation of the test setup. It simulates the propagation of the photons through the bar, taking into account the wavelength dependencies of both the photon absorption in the quartz bar and the quantum efficiency of the PMT. The surface reflectivity is taken to be 0.9995. The number of photo-electrons can be written using the "Cherenkov quality factor" N_0 as

$$N_{pe} = \epsilon_{coll} \frac{d}{cos\theta_D} N_0 sin^2\theta_c, \qquad (1)$$

[3]Burle Industries, Inc., 1000 New Holland Ave., Lancaster, PA 17601, U.S.A.

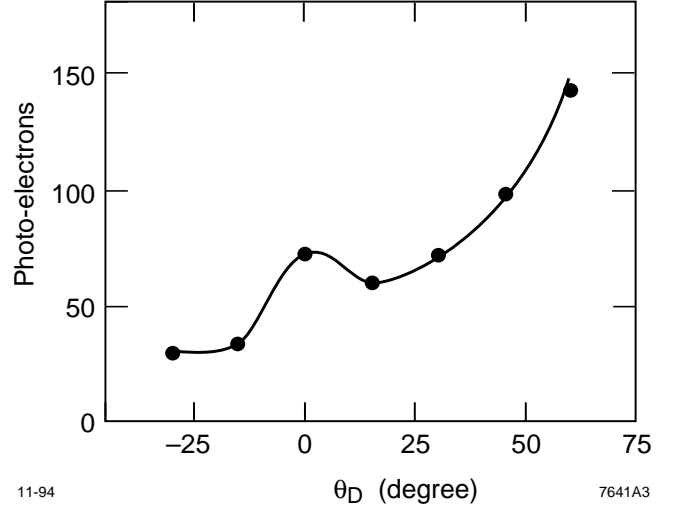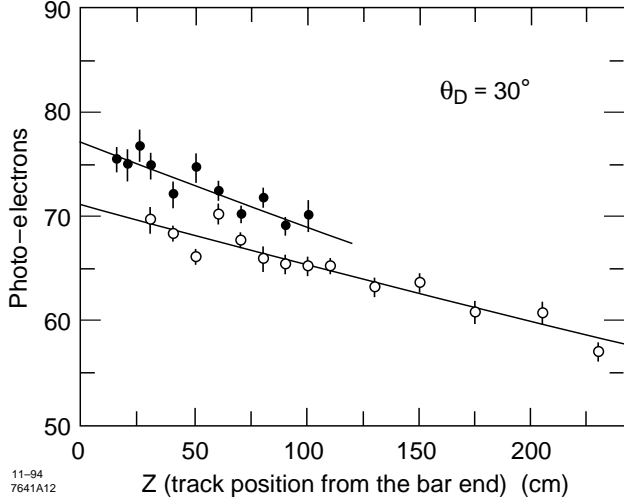[4]Thorn EMI Electron Tubes, Bury Street, Ruislip, Middlesex, HA4 7TA, U.K.

Figure 6: Track position dependence of the photo-electron yield at a dip angle $\theta_D = 30°$. The solid circles are measurements with the 120 cm long bar and the open circles are with the 240 cm long bar. The solid lines are exponential fits to the data with an effective attenuation rate of 11.2 %/m and 8.7 %/m, respectively.
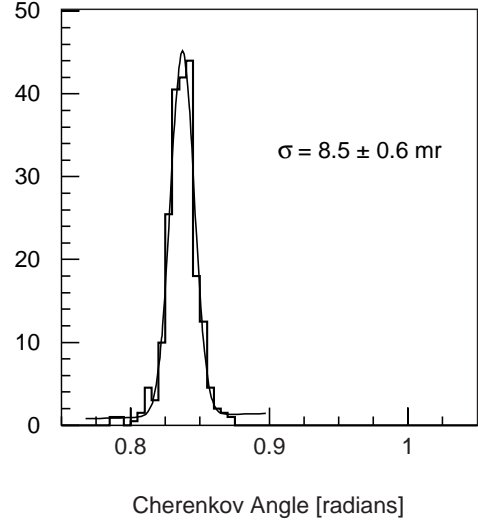
Figure 7: Single Cherenkov photon angle distribution at $\theta_D = 30°$, l=90 cm, and $z = 205$ cm with the 240 cm long bar. The line is a fit of a Gaussian plus polynomial to the data. The width of the fit is 8.5±0.6 mr.

where ϵ_{coll} is the photon collection efficiency, θ_c is the Cherenkov angle, d is the thickness of the radiator bar, and θ_D is the dip angle of the track. The collection efficiency ϵ_{coll} is a function of dip angle, track position, and photon energy. The N_0 is given by

$$N_0 = \frac{\alpha}{\hbar c} \int \epsilon_{PMT} dE, \qquad (2)$$

where ϵ_{PMT} is the quantum efficiency of the PMT and E is the photon energy. From the quantum efficiency curve claimed by the manufacturer, we find $N_0 \sim 150$ cm^{-1} [‡]. The Monte-Carlo simulation well reproduces both the dip angle dependence and absolute yield. The bump at $\theta_D = 0°$ is due to the fact that all of the photons are trapped in the bar at this angle, and the photons travelling away from the PMT can reflect from the other end of the bar.

Fig. **??**. shows the number of photo-electrons as a function of track position along the bar measured at a dip angle $\theta_D = 30°$. The solid circles are the measurements of the 120 cm long bar and the open circles are of the 240 cm long bar. The solid lines are exponential fits to the data points. Since the absorption length and the surface reflectivity are both wavelength dependent, and the path length of the photons depends on the initial direction of the photons, the position dependence will not be a simple exponential function, and it is difficult to deduce the absorption length and

the reflectivity separately from the measurement. However, a simple exponential curve as a function of the track position z is a good approximation if the photon absorption length is long and the reflectivity is close to 1. The fitted "effective attenuation rates" are 11.2±1.9 %/m with 77.0±0.9 photo-electrons at $z = 0$ for the 120 cm long bar, and 8.7±0.6 %/m with 71.1±0.5 photo-electrons at $z = 0$ for the 240 cm long bar. These attenuation rates are consistent with each other. The photo-electron yield difference at $z = 0$ is consistent with the cathode blue sensitivities of the PMTs claimed by the manufacturer (10.0 and 9.7 μA/lm) and the calibration error ($\sim$3 %). No significant light loss at the glue joint in the 240 cm long bar was seen in this measurement.

B. *Single Cherenkov Photon Angle Resolution*

We measured the single Cherenkov photon angle resolution with the PMT array at various stand-off distances l, dip angles θ_D, and track positions z. The array was placed with an offset in the y-direction and no offset in the x-direction, so that it covered the central part of the image, where the photon population was the largest (see Fig. **??** for the coordinate system). The y-offset varied with the dip angle θ_D as the image moved. Fig. **??** shows the single Cherenkov photon angle distribution at a dip angle $\theta_D = 30°$, track position $z = 205$ cm, and stand-off distance $l = 90$ cm with the 240 cm long bar. The solid line is a fit of a Gaussian plus polynomial to the data. The width of the Gaussian part is $\sigma = 8.5 \pm 0.6$ mr.

Table **??** shows the expected major contributions to the angular resolution. The geometrical term (a) is due to the

---

[‡]This is different from the number quoted in [**?**], which uses different definitions for N_0 and ϵ_{coll}.

stand-off distance l	90 cm	
track dip angle θ_D	30°	60°
a) geometrical	4.9 mr	4.3 mr
b) chromatic dispersion	4.2 mr	7.2 mr
c) momentum distribution	1.6 mr	
d) multiple scattering	1.5 mr	2.1 mr
e) tracking error	2 mr	
f) reconstruction error	3.1 mr	4.7 mr
total	7.8 mr	10.2 mr

Table 1: Contributions to the single Cherenkov photon angle resolution at $l = 90$ cm, and $\theta_D = 30°$ and $60°$.

			resolution [mr]	
θ_D	l [cm]	z [cm]	measurement	estimate
30°	60	60	10.1 ± 1.1	10.1
40°	60	60	11.7 ± 1.2	12.0
50°	60	60	14.0 ± 0.9	12.8
60°	60	60	12.6 ± 0.8	12.5
60°	90	30	8.6 ± 1.4	10.2
30°	90	30	8.5 ± 0.5	7.8
30°	90	110	7.5 ± 1.2	7.8
30°	90	205	8.5 ± 0.6	7.8

Table 2: Summary of the single Cherenkov photon resolution measurements. The measurement at $z = 205$ cm is for the 240 cm long bar. All others are for the 120 cm long bar.

granularity of the photon detector (2.3 cm diameter) and the bar size (1.7 cm thick). It is approximately given by

$$\delta\theta_{geo} \approx \frac{n_2}{n_1} \frac{l}{l^2 + l_y^2} \sqrt{\delta y_{PMT}^2 + \delta y_{bar}^2}, \qquad (3)$$

where δy_{PMT} and δy_{bar} are the spatial resolution in the y-direction of the PMT and bar, respectively, and l_y is the array offset in the y-direction. Only the y-direction is relevant in this prototype test, since the array is placed at the central part of the image, where it is flat in the x-direction (see Fig. **??**). The factor n_2/n_1 is due to the refraction at the bar end. The chromatic dispersion (b) is due to the wavelength dependence of the refractive index of the radiator n_1. The chromatic contribution at Cherenkov photon production is estimated to be 5.4 mr [**?**]. This is the fundamental limitation on the performance. There is also a chromatic effect on the refraction angle at the bar end. This effect contributes coherently with the chromatic error at production. It increases the total chromatic contribution at larger dip angles and reduces it at smaller dip angles. However, if water is used as the stand-off material instead of air, it will be negligible because the wavelength dependence of the index of water is very similar to that of quartz. The reconstruction error (f) is due to the left-right ambiguity of the image. It is only significant near the central part of the image, where the images from the left and right side of the bar overlap (see Fig. **??**), and is negligible for most of the photons in a full scale device.

Another possible contribution is the resolution smearing during the transport along the bar. Imperfections of the bar shape (e.g. non-parallelisim or non-flatness of the surfaces, or non-squareness of the bar cross-section) would cause emittance growth. However, the DIRC needs an accuracy of only ~ 1 mr and the quality of the bars being used exceeds this requirement, so this effect is negligible.

The expected total resolution, including momentum distribution of the tracks (c) ($p_\mu \geq 1$ GeV/c); multiple scattering (d) (including 2 mm thick aluminum wall of the light-box); and tracking error (e), is 7.8 mr at $\theta_D = 30°$ and 10.2 mr at $\theta_D = 60°$ for $l = 90$ cm.

Table **??** is a summary of the measurements. They are consistent with the estimates. No significant dependence on the track position z was observed, and no effect of the glue joint could be seen.

V.   Conclusions

We have measured the Cherenkov photo-electron yield and the single Cherenkov photon resolution at various track dip angles and track positions along the quartz bars. The dip angle dependence of the photo-electron yield is well reproduced by a detailed Monte-Carlo simulation. The photon attenuation rate along the bar is ~ 10 %/m for track dip angle $\theta_D = 30°$. These photo-electron yield and photon attenuation rate are adequate for a full scale device with ~ 5 m long quartz bars [**?**]. The measured single Cherenkov photon resolution is consistent with the estimate and no significant dependence on the track position has been seen. No significant light loss or resolution loss at the glue joint in the 240 cm long bar has been seen.

In conclusion, all measurements are consistent with each other and with our Monte-Carlo simulation and estimates. They demonstrate the particle identification capability of the DIRC, and show that the main features of the device are well-understood and that the performance can be safely extrapolated to a full scale device.

References

[1] SLAC-REP-373 (1991);
    SLAC-REP-419 (1993).

[2] SLAC-REP-443 (1994).

[3] P. Coyle *et al.*, SLAC-PUB-5594 (1991);
    B. Ratcliff, SLAC-PUB-5853 (1992).

[4] B. Ratcliff, SLAC-PUB-5946 (1992);
    B. Ratcliff, SLAC-PUB-6047 (1993).

[5] P. Coyle *et al.*, SLAC-PUB-6371 (1993).